
Membrane Transport, Structure, Function, and Biogenesis:

# Dynamic Regulation of Cystic Fibrosis Transmembrane Conductance Regulator by Competitive Interactions of Molecular Adaptors

Ji Hyun Lee, Wito Richter, Wan Namkung, Kyung Hwan Kim, Eunjoon Kim, Marco Conti and Min Goo Lee

*J. Biol. Chem. 2007, 282:10414-10422.*
*doi: 10.1074/jbc.M610857200 originally published online January 23, 2007*

THE JOURNAL OF BIOLOGICAL CHEMISTRY VOL. 282, NO. 14, pp. 10414–10422, April 6, 2007


# Dynamic Regulation of Cystic Fibrosis Transmembrane Conductance Regulator by Competitive Interactions of Molecular Adaptors*

Received for publication, November 24, 2006, and in revised form, January 16, 2007 Published, JBC Papers in Press, January 23, 2007, DOI 10.1074/jbc.M610857200

**Ji Hyun Lee[‡], Wito Richter[§], Wan Namkung[‡], Kyung Hwan Kim[‡], Eunjoon Kim[¶], Marco Conti[§], and Min Goo Lee[‡1]**

*From the [‡]Department of Pharmacology, Institute of Gastroenterology, Yonsei University College of Medicine, Seoul 120-752, Korea, [§]Division of Reproductive Biology, Department of Obstetrics and Gynecology, Stanford University School of Medicine, Stanford, California 94305-5317, and [¶]Creative Research Center for Synaptogenesis and Department of Biological Sciences, Korea Advanced Institute of Science and Technology, Daejeon 305-701, Korea*

**Disorganized ion transport caused by hypo- or hyperfunctioning of the cystic fibrosis transmembrane conductance regulator (CFTR) can be detrimental and may result in life-threatening diseases such as cystic fibrosis or secretory diarrhea. Thus, CFTR is controlled by elaborate positive and negative regulations for an efficient homeostasis. It has been shown that expression and activity of CFTR can be regulated either positively or negatively by PDZ (PSD-95/discs large/ZO-1) domain-based adaptors. Although a positive regulation by PDZ domain-based adaptors such as EBP50/NHERF1 is established, the mechanisms for negative regulation of the CFTR by Shank2, as well as the effects of multiple adaptor interactions, are not known. Here we demonstrate a physical and physiological competition between EBP50-CFTR and Shank2-CFTR associations and the dynamic regulation of CFTR activity by these positive and negative interactions using the surface plasmon resonance assays and consecutive patch clamp experiments. Furthermore whereas EBP50 recruits a cAMP-dependent protein kinase (PKA) complex to CFTR, Shank2 was found to be physically and functionally associated with the cyclic nucleotide phosphodiesterase PDE4D that precludes cAMP/PKA signals in epithelial cells and mouse brains. These findings strongly suggest that balanced interactions between the membrane transporter and multiple PDZ-based adaptors play a critical role in the homeostatic regulation of epithelial transport and possibly the membrane transport in other tissues.**

The cystic fibrosis transmembrane conductance regulator (CFTR)[2] is a $Cl^-$ channel and a key regulator of fluid and ion transport in the gastrointestinal, respiratory, and genitourinary epithelia (1, 2). Hypofunctioning of CFTR due to genetic defects causes cystic fibrosis, the most common lethal genetic disease in Caucasians (3, 4), whereas hyperfunctioning of CFTR resulting from various infections evokes secretory diarrhea (5), the leading cause of mortality in early childhood in the world (World Health Organization statistics). Therefore, maintaining and regulating a dynamic balance between CFTR-activating and CFTR-inactivating machineries is an important mechanism for maintaining body homeostasis.

Accumulating evidence suggests that protein-protein interactions play a critical role in the regulation of CFTR and other epithelial transporters (6–8). PDZ (PSD-95/discs large/ZO-1) domain-based adaptors, best studied in the postsynaptic density (PSD) region of neurons, have emerged as a large group of proteins that sequester functionally related groups of transporters, receptors, and other effector proteins into integrated molecular complexes (9, 10). Epithelial cells also utilize specific PDZ proteins to direct the polarized activities in their apical and basolateral membranes. Recently we reported functional and physical associations between the PDZ domain-containing protein Shank2 and two epithelial transporters, CFTR and the $Na^+/H^+$ exchanger 3 (NHE3) (11, 12). Interestingly Shank2 attenuated the cAMP-dependent regulation of CFTR and NHE3. Conversely it has been shown that PDZ domain-based adaptors, such as EBP50/NHERF1 and E3KARP/NHERF2, can enhance the effects of cAMP on these transporters by recruiting a cAMP-dependent protein kinase (PKA)/PKA-anchoring protein (AKAP) complex (13, 14). Physiological significance of these adaptors in the regulation of CFTR function has also been verified in many other studies (6). For example, recent evidence demonstrates that native CFTR and EBP50 are co-immunoprecipitated in human airway epithelial cells (15) and that CFTR-dependent anion current is reduced in the intestine of EBP50 knock-out mice (6).

The PDZ domain of Shank proteins has a three-dimensional structure very similar to the PDZ domains of EBP50/NHERF1 (16). In particular, these PDZ domains all contain a negatively charged amino acid at the end of the $\beta$ C strand of the PDZ

* This work was supported by Grant R02-2004-000-10091-0 from the Korea Research Foundation, Ministry of Education and Human Resources Development, Korea and Grant 03-PJ10-PG13-GD01-0002 from the Korea Health 21 R&D Project, Ministry of Health and Welfare, Korea (to M. G. L.) and National Institutes of Health Grant HD20788 (to M. C.). The costs of publication of this article were defrayed in part by the payment of page charges. This article must therefore be hereby marked "*advertisement*" in accordance with 18 U.S.C. Section 1734 solely to indicate this fact.

[1] To whom correspondence should be addressed: Dept. of Pharmacology, Yonsei University College of Medicine, 134 Sinchon-Dong, Seoul 120-752, Korea. Tel.: 82-2-2228-1737; Fax: 82-2-313-1894; E-mail: mlee@yumc.yonsei.ac.kr.

[2] The abbreviations used are: CFTR, cystic fibrosis transmembrane conductance regulator; AKAP, cAMP-dependent protein kinase-anchoring protein; IBMX, 3-isobutyl-1-methylxanthine; IP, immunoprecipitation; NHE, $Na^+/H^+$ exchanger; NTA, $Ni^{2+}$-nitrilotriacetic acid; PDE, phosphodiesterase; PKA, cAMP-dependent protein kinase; PDZ, PSD-95/discs large/ZO-1; PSD, postsynaptic density; SPR, surface plasmon resonance; CHO, Chinese hamster ovary; GST, glutathione *S*-transferase; PR, proline-rich; UCR, upstream conserved region.

domain structures ($Glu^{43}$ in hEBP50, $Asp^{634}$ in rShank1, and $Asp^{80}$ in hShank2) that preferentially interacts with a positively charged residue at the −1 position in the C terminus of the membrane transporters, such as −T**R**L in CFTR. Therefore, the question arises whether EBP50 and Shank2 have distinct CFTR binding sites or mutually compete for binding of a single site in cells expressing both adaptor proteins.

In the present study, we determined the kinetic properties and physiological significance of the interactions between CFTR and the PDZ-based adaptors EBP50 and Shank2. Using surface plasmon resonance (SPR) assays, we found that the dissociation constant ($K_D$) of CFTR-Shank2 binding was similar to that of CFTR-EBP50 binding and that both proteins apparently compete for binding at the same site. Consecutive patch clamp studies revealed that CFTR $Cl^-$ channel activity was dynamically regulated by the competition of Shank2 and EBP50 binding. Notably in contrast to the PKA/AKAP recruitment by EBP50 (6), Shank2 was found to tether PDE4D to the CFTR complex, thus attenuating cAMP/PKA signals. Our results suggest that the competitive balance between Shank2 and EBP50 binding to the CFTR channel may maintain homeostatic regulation of epithelial ion and fluid transport.

## EXPERIMENTAL PROCEDURES

*Cell Cultures and Plasmid Vectors*—NIH 3T3 and COS7 cells were maintained in Dulbecco's modified Eagle's medium supplemented with 10% fetal calf serum. T84 cells were purchased from the American Type Culture Collection (ATCC CCL-248) and maintained in a 1:1 mixture of Ham's F-12 medium and Dulbecco's modified Eagle's medium supplemented with 5% fetal bovine serum. CHO-K1 cells (KCLB 10061; Korea Cell Line Bank, Seoul, Korea) were maintained in RPMI 1640 medium supplemented with 10% fetal bovine serum. The pcDNA3.1-rShank2/CortBP1 (17), pcDNA3.1-hEBP50/NHERF-1 (12), and pCMV5 vectors containing rPDE4D1 to rPDE4D9 have been described previously (18).

*SPR Measurements and Kinetic Analysis of Sensorgrams*—PDZ1-(1–139), PDZ2-(132–299), and PDZ1+2-(1–299) domains of hEBP50/NHERF1 and the PDZ domain of rShank2/CortBP1-(1–142) were PCR-amplified and cloned into the pRSET A vector (Invitrogen) to create His-tagged constructs. The C-terminal 29 amino acid residues of hCFTR (GenBank™ accession number NM_000492) and PDZ1+2 of hEBP50 (for competition assay, see Fig. 1*D*) were PCR-amplified and cloned into the pGEX-4T-1 vector (Amersham Biosciences) to create GST fusion constructs. All constructs were confirmed by sequence analysis. All fusion proteins were expressed in *Escherichia coli* BL21 (DE3) cells and purified on $Ni^{2+}$-nitrilotriacetic acid (NTA) resin (Qiagen, Venlo, The Netherlands) and glutathione-Sepharose 4B (Amersham Biosciences) as appropriate. The purified proteins were quantified using Bio-Rad protein assay reagent, and their purity was assessed as >90% by Coomassie staining of SDS-PAGE gels. An SPR system equipped with an NTA chip (BIAcore 3000; Biacore AB, Uppsala, Sweden) was used to capture His-tagged PDZ fusion proteins. Analytes (GST-tagged proteins) at various concentrations in HEPES-buffered saline-EP (0.01 M HEPES, 0.15 M NaCl, 50 μM EDTA, 0.005% Tween 20, pH 7.4) were perfused at a flow rate of 30 μl/min. The sensor chip was regenerated between each analysis using successive injections of solutions containing 0.15 M NaCl and 0.35 M EDTA. Response curves were generated by subtracting the background signal generated simultaneously by the control flow cell. Background-subtracted curves were prepared for fitting by subtracting the signal generated by buffer alone on experimental flow cells. Sensorgram curves and kinetic parameters were evaluated by the BIAevaluation 3.1 software (Biacore AB), which uses numerical integration algorithms.

*Measurement of $Cl^-$ Channel Activities*—Whole-cell recordings were performed on CFTR-transfected CHO-K1 cells as reported previously (19). The pipette solution contained 140 mM *N*-methyl D-glucamine chloride (NMDG-Cl), 5 mM EGTA, 1 mM $MgCl_2$, 1 mM Tris-ATP, and 10 mM HEPES (pH 7.2), and the bath solution contained 140 mM *N*-methyl D-glucamine chloride, 1 mM $CaCl_2$, 1 mM $MgCl_2$, 10 mM glucose, and 10 mM HEPES (pH 7.4). All experiments were performed at room temperature (22–25 °C). After establishing the whole-cell configuration, CFTR was activated by adding forskolin and/or 3-isobutyl-1-methylxanthine (IBMX). The holding potential used was −30 mV, and the current output was filtered at 5 kHz. Currents were digitized and analyzed using an AxoScope 8.1 system and a Digidata 1322A analog/digital converter (Axon Instruments, Union City, CA).

Single channel activity of CFTR was measured in inside-out configurations using fire-polished pipettes with a resistance of 20–25 megaohms. The pipette solution contained 140 mM NaCl, 5 mM KCl, 1 mM $MgCl_2$, 1 mM $CaCl_2$, and 10 mM HEPES (pH 7.4), and the bath solution contained 140 mM NaCl, 5 mM KCl, 1 mM $MgCl_2$, and 10 mM HEPES (pH 7.4). Following patch excision, channels were activated by adding the catalytic subunit of PKA (40 unit/ml; Promega, Madison, WI) and 1 mM MgATP. After channel activation, EBP50 and/or Shank2-PDZ at desired concentrations was added to the bath. Holding voltage used in the single channel recording was +60 mV. The pCLAMP software package (version 9.2, Axon Instruments) was used for data acquisition and analysis. The voltage and current data were low pass-filtered at 1 kHz during the recordings, and the single channel data were further digitally filtered at 25 Hz. The number of active channels in a patch was determined from the number of simultaneously open channels during at least 15 min of recording.

*Reverse Transcription-PCR*—Reverse transcription-PCR analysis was performed to identify the phosphodiesterase (PDE) isoforms in NIH 3T3 cells and T84 cells using protocols reported previously (12). The primer sequences specific to PDE3 and PDE4 were selected from regions common to both mouse and human PDEs: 1) PDE3A: sense, CAC AGG GCC TTA ACT TAC AC; antisense, TTG AGT CCA GGT TAT CCA TGA C; PCR product, 370 bp; 2) PDE3B: sense, CAG GAA GGA TTC TCA GTC AGG; antisense, GTC ATT GTA TAA AAC TGC CTG AGG; PCR product, 464 bp; 3) PDE4A: sense, ATC AAC ACC AAT TCG GAG C C; antisense, TCA CCC TGC TGG AAG AAC TC; PCR product, 398 bp; 4) PDE4B: sense, AGT CCT TGG AAT TGT ATC GG; antisense, CTG GAT CAA TCA CAC AAA GCG TC; PCR product, 432 bp; 5)

PDE4C: sense, TTC CAG ATC CCA GCA GAC AC; antisense, ATG ACC ATC CTG CGC AGA CTC; PCR product, 392 bp; and 6) PDE4D: sense, GCC AAG GAA CTA GAA GAT GTG; antisense, CAT CAT GTA TTG CAC TGG C; PCR product, 328 bp.

*Immunoprecipitation (IP), Immunoblotting, and Immunohistochemistry*—CHO-K1, COS-7, T84 cells, and rat cerebellum were lysed with lysis buffer (20 mM HEPES, pH 7.4, 200 mM NaCl, 5 mM EDTA, 1% Triton X-100, 1 mM $NaVO_4$, and 1 mM β-glycerophosphate) containing Complete protease inhibitor mixture (Roche Applied Science). After lysis, cell debris were removed by centrifugation, and cleared lysates were mixed with the appropriate antibodies and incubated overnight at 4 °C. Immune complexes were collected by incubation for 2 h at 4 °C with protein A/G PLUS-agarose and washed four times with lysis buffer prior to electrophoresis. The immunoprecipitates and cell lysates were suspended in 2× SDS sample buffer and boiled for 5 min and then separated by SDS-PAGE. The separated proteins were transferred to nitrocellulose membranes, and the membranes were blocked by incubation for 1 h in a solution containing 5% nonfat dry milk in 20 mM Tris-HCl, pH 7.5, 150 mM NaCl, and 0.05% Tween 20. The membranes were then incubated with the appropriate primary and secondary antibodies, and protein bands were detected with enhanced chemiluminescence solutions. Rabbit polyclonal antibodies anti-Shank2 1136 (17) and anti-PDE4D5 α-4D5 (18) and the mouse monoclonal pan-PDE4D antibody M3S1 (20) were described previously. Rabbit polyclonal pan-PDE4D antibody ab14613 was purchased from Abcam Inc., Cambridge, UK.

Immunostaining of frozen sections was performed as reported previously (12). Briefly colon tissues from Sprague-Dawley rats were embedded in OCT (Miles, Elkhart, IN), frozen in liquid $N_2$, and cut into 4-μm sections. The sections were stained by incubation with polyclonal anti-Shank2 1136 and monoclonal anti-pan-PDE4D M3S1 antibodies followed by appropriate secondary antibodies tagged with fluorophores. Images were obtained with a Zeiss LSM 510 confocal microscope.

*GST Pulldown Assay*—Regions corresponding to residues of rShank2 PDZ-(1–142), proline-rich (PR)-(134–1176), and sterile α motif-(1164–1253) domains were PCR-amplified and cloned into pGEX-4T-1 vector (Amersham Biosciences) to create GST fusion constructs. Shank2 PR domains were further dissected, and two GST fusion constructs were generated: PR1-(134–669) and PR2-(647–1176). All fusion proteins were expressed in *E. coli* BL21 (DE3) and purified with glutathione-Sepharose 4B (Amersham Biosciences). For pulldown assays, CHO cells were lysed on ice in a 1% Triton X-100 buffer containing 150 mM NaCl, 2 mM $MgCl_2$, 2 mM $CaCl_2$, 10 mM HEPES, pH 7.4, and proteinase inhibitors (CompleteMini, Roche Applied Science). Debris was removed by centrifugation, and 100 μl of lysate supernatants were supplemented with 900 μl of buffer prior to addition of 10 μg of each GST fusion protein. Following overnight incubation at 4 °C, samples were supplemented with 80 μl of glutathione-Sepharose (Amersham Biosciences) and incubated for an additional 4 h at 4 °C. The glutathione-Sepharose was pelleted and washed (3 × 5 min) at 4 °C with wash buffer (phosphate-buffered saline containing 0.1% Triton X-100 and 100 mM β-mercaptoethanol) prior to resuspension in SDS sample buffer and SDS-PAGE.

*Measurements of PDE Activity*—Whole brain tissues from wild type and PDE4D knock-out mice (21) were lysed in buffer containing 50 mM HEPES, pH 7.4, 250 mM NaCl, 10% glycerol, 0.5% Nonidet P-40, 1 mM EDTA, 0.2 mM EGTA, 10 mM NaF, 10 mM $Na_4P_2O_7$, 1 μM microcystin, 2 mM 4-(2-aminoethyl) benzenesulfonylfluoride, and a mixture of protease inhibitors. Cell lysates were centrifuged at 14,000 × *g*, and supernatants were immunoprecipitated using 5 μl of anti-Shank2 antibody coupled to 25 μl of protein G-Sepharose for 4 h. After centrifugation, pellets were washed three times, and PDE activity was then measured as described previously (18). In brief, samples were assayed in a reaction mixture of 200 μl containing 40 mM Tris-HCl, pH 8.0, 10 mM $MgCl_2$, 5 mM β-mercaptoethanol, 1 μM cAMP, 0.75 mg/ml bovine serum albumin, and 0.1 μCi of [$^3$H]cAMP for 10 min at 33 °C. The reaction was terminated by the addition of 200 μl of 10 mM EDTA in 40 mM Tris-HCl, pH 8.0, followed by heat inactivation in a boiling water bath for 1 min. The PDE reaction product 5′-AMP was then hydrolyzed by incubation of the assay mixture with 50 μg of *Crotalus atrox* snake venom for 20 min at 33 °C. The resulting adenosine was separated by anion exchange chromatography using 1 ml of AG1-X8 resin and quantitated by scintillation counting.

## RESULTS

*Shank2 and EBP50 Compete for Binding on CFTR*—To understand the dynamics of CFTR positive and negative regulations, we determined the binding kinetics of the association between CFTR and the PDZ domains of EBP50 and Shank2 using SPR analyses (Fig. 1). As EBP50 has two PDZ domains, three His-tagged proteins, PDZ1-(1–139), PDZ2-(132–299), and PDZ1+2-(1–299), were used to analyze their kinetics separately. His-tagged PDZ domains were captured on NTA chips, and their binding to the GST-tagged C terminus of CFTR was sensored by SPR. As shown in the sensorgrams, the PDZ domains of Shank2 and EBP50 specifically bind the C terminus of CFTR in a dose-dependent fashion (Fig. 1, *A* and *B*). The overall dissociation constants at the equilibrium state ($K_D$ values) of Shank2 PDZ and EBP50 PDZ1+2 were within comparable ranges at the tens of nanomolar levels (Fig. 1*C*). Interestingly EBP50 PDZ1+2 has approximately a 1 order of magnitude faster association ($K_a$) and dissociation ($K_d$) kinetics than Shank2 PDZ. Further analyses of EBP50 PDZs using separate PDZ1 and PDZ2 proteins revealed that the overall EBP50 binding to CFTR is driven by PDZ1, which has a ~3 times higher affinity than PDZ2 (Fig. 1*C*). A solution competition assay was performed to examine the possibility of mutual competition between the PDZs of Shank2 and EBP50 in binding to CFTR. After capturing His-tagged Shank2 PDZ on NTA chips, the SPR system was perfused with a fixed dose of the C terminus of CFTR (300 nM) and increasing doses of GST-tagged EBP50 PDZ1+2. Importantly the addition of EBP50 PDZs dose-dependently decreased the association between Shank2 PDZ and CFTR with an $IC_{50}$ value of 91 nM (Fig. 1*D*).

*Regulation of CFTR $Cl^-$ Channel Activity by CFTR-EBP50 and CFTR-Shank2 Competitions*—The above results imply that Shank2 and EBP50 compete for binding on CFTR. This com-

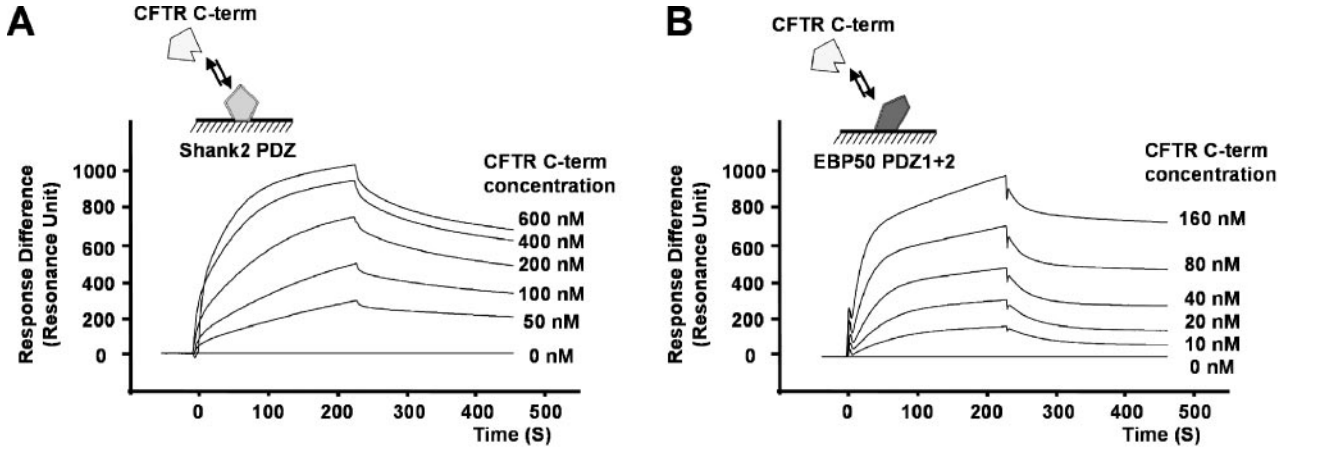


C

| Ligand | Analyte | Ka ($M^{-1}s^{-1}$) | Kd ($s^{-1}$) | KD (Kd/Ka, M) |
|---|---|---|---|---|
| Shank2 PDZ | CFTR C-term | $3.07x10^{4}$ | $1.73x10^{-3}$ | $5.63x10^{-8}$ |
| EBP50 PDZ1+2 | CFTR C-term | $4.89x10^{5}$ | $1.10x10^{-2}$ | $2.24x10^{-8}$ |
| EBP50 PDZ1 | CFTR C-term | $2.56x10^{5}$ | $5.85x10^{-3}$ | $2.29x10^{-8}$ |
| EBP50 PDZ2 | CFTR C-term | $7.72x10^{4}$ | $5.71x10^{-3}$ | $7.39x10^{-8}$ |

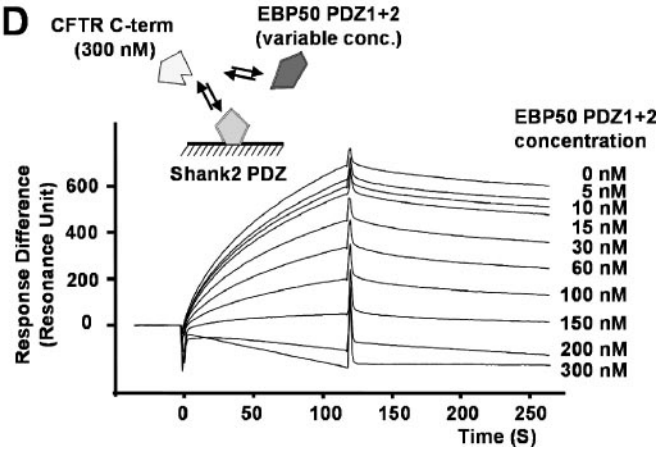


FIGURE 1. **Interactions between CFTR and PDZ-based adaptors determined by SPR assays.** *A* and *B*, sensorgrams showing the interaction between the C terminus of CFTR and the PDZ domains of Shank2 and EBP50/NHERF1. His-tagged PDZ domains of Shank2 and EBP50 were captured on NTA chips, which were then perfused with various concentrations of a peptide encoding the C-terminal 29 amino acids of CFTR. *C*, binding kinetics of the interaction between CFTR and the PDZ domains of Shank2 and EBP50. Values shown represent the average of two experiments each performed in duplicate. *D*, sensorgram of a solution competition assay between CFTR-Shank2 PDZ and CFTR-EBP50 PDZ1+2 interactions. After capturing His-tagged Shank2 PDZ, the NTA chips were perfused with a fixed concentration of the C terminus of CFTR (300 nM) and increasing concentrations of the GST-tagged EBP50 PDZ1+2. EBP50 PDZ1+2 dose-dependently decreased the CFTR-Shank2 PDZ association with an $IC_{50}$ value of 91 nM ($n = 3$). $K_a$, association constant; $K_d$, dissociation constant; $K_D$, overall dissociation constant at equilibrium status ($K_d/K_a$).

petitive balance may affect CFTR ion transporting activities at the apical membrane of intestine, pancreas, and kidney epithelia, where Shank2 and EBP50 are abundantly expressed (7, 12). We therefore determined the effects of the competition between EBP50 and Shank2 PDZ binding on the CFTR $Cl^-$ channel activity using inside-out configurations (Fig. 2). Following patch excision from CFTR-transfected CHO cells, patch membranes were washed with a high bath flow for 5 min to eliminate endogenous activation. When CFTR was activated by the addition of the catalytic subunit of PKA and ATP to the bath solution, an ion channel activity with a single channel conductance of 7.1 ± 0.3 picosiemens and a linear current-voltage relationship was evoked that was absent in mock-transfected cells. It has been shown that adaptors with multiple PDZ domains, such as EBP50 and CAP70/PDZK1, can activate CFTR $Cl^-$ channel activity independently of cAMP signals by altering protein conformation including multimerization (23, 24). In agreement with these reports, treatment with EBP50 (100 nM) induced a 2.8-fold increase in the open probability ($P_o$) of CFTR. Importantly addition of Shank2 PDZ (300 nM) inhibited the EBP50-induced increase in CFTR $P_o$ by 75 ± 8% (Fig. 2, *A* and *C*). The effect of Shank2 PDZ *versus* EBP50 competition was then examined in reverse order. Shank2 PDZ treatment alone did not evoke significant changes in CFTR $P_o$ at basal levels; however, it greatly inhibited the CFTR activation mediated by EBP50. Addition of EBP50 induced only a minor increase in CFTR $P_o$ after Shank2 pretreatment (Fig. 2, *B* and *D*). When performing the above experiments using EBP50 PDZ1+2, which does not bind AKAPs due to the lack of the ezrin-radixin-mosesin (ERM) domain, we obtained results similar to those using the entire EBP50 protein (Fig. 2, *C* and *D*).

These findings indicate that Shank2 can reversibly inhibit the EBP50-induced CFTR activation by competing with EBP50 for binding at the C terminus of CFTR and hence by breaching the EBP50-induced active conformation of CFTR. However, this does not explain the observation that Shank2 inhibits the cAMP-induced phosphorylation and activation of CFTR in living cells. In CFTR-expressing NIH 3T3 cells, it has been shown that Shank2 overexpression decreased CFTR channel activity and phosphorylation induced by the adenylyl cyclase activator forskolin (12). It is well known that CFTR is primarily activated by phosphorylation of the R-domain by PKA (2). Recruitment

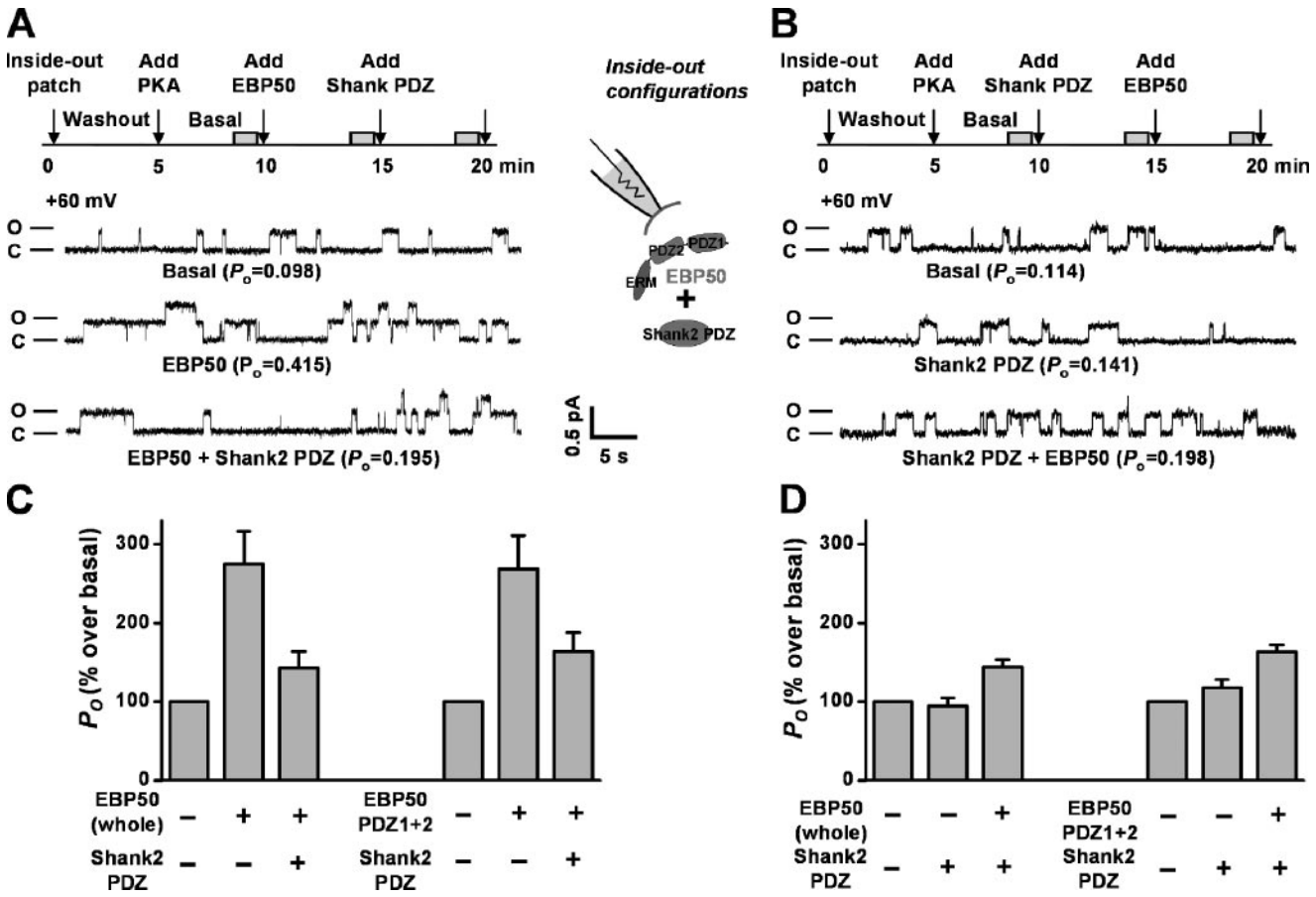


FIGURE 2. **Regulation of CFTR single channel activity by a competition between CFTR-EBP50 and CFTR-Shank2 PDZ binding.** CFTR $Cl^-$ channel activity was measured in CFTR-transfected CHO cells with inside-out configurations. Current records at +60 mV were analyzed to estimate the $P_o$. *A*, after a 5-min wash of patch membranes, CFTR was activated by addition of PKA. Solutions containing EBP50 (100 nM) with and without Shank2 PDZ (300 nM) were perfused to the bath chamber at 5-min intervals. $P_o$ was calculated from the recording of the last 1 min of each 5-min interval. Similar experiments were performed with EBP50 PDZ1+2, which lacks the AKAP/PKA-binding ezrin-radixin-moesin (ERM) domain, instead of EBP50 (*whole*). A summary of five experiments with EBP50 and three experiments with EBP50 PDZ1+2 is presented in *C*. *B*, the effect of Shank2 PDZ and EBP50 binding on CFTR activity was examined in reverse order of *A* with Shank2 PDZ treatment preceding the EBP50 treatment. A summary of five experiments with EBP50 and three experiments with EBP50 PDZ1+2 is presented in *D*. *O*, open; *C*, closed.

by Shank2 of cyclic nucleotide PDEs, which attenuate cAMP signals, or phosphatases, which offset the action of PKA, might explain these findings. The latter is unlikely, however, because CFTR phosphorylation was decreased in the Shank2-transfected cells even in the presence of a high concentration of the nonspecific phosphatase inhibitor $NaVO_4$ (12).

*Shank2 Associates with PDE4D*—An important clue was obtained in an experiment with the non-selective PDE inhibitor IBMX (Fig. 3, *A–D*). Stimulation of CFTR-expressing CHO cells with 3 $\mu$M forskolin induced a CFTR $Cl^-$ current that is dependent on the presence of $Cl^-$ in bath and pipette solutions, is inhibited by 5-nitro-2-(3-phenylpropylamino)benzoate, and has linear current-voltage relationships in whole-cell configurations. However, when Shank2 was co-expressed, the same amount of forskolin produced very small or no CFTR currents. Interestingly additional treatment with IBMX evoked a robust CFTR current in Shank2-expressing cells, although its peak amplitude was still 56 ± 7% that of mock-transfected cells (Fig. 3, *A* and *B*).

These results suggest a functional association between the PDE activity and the Shank2-mediated inhibition of CFTR. We next identified the PDE subtypes involved and determined whether Shank2 directly interacts with PDEs. Of the 11 PDE families, PDE3 and PDE4 are strong candidates for Shank2 association as they are sensitive to IBMX and are known to be expressed in epithelial cells (25). The PDE3 family consists of two genes, 3A and 3B, and the PDE4 family consists of four, 4A–4D. Reverse transcription-PCR results using primers specific to the common regions of mouse and human PDEs revealed that several PDE3 and PDE4 genes, including PDE3A, -4A, and -4D, are expressed in mouse fibroblast NIH 3T3 cells and human colonic T84 cells (Fig. 3*E*). As both PDE3 and PDE4 are expressed, the patch clamp experiment shown in Fig. 3*B* was repeated after pretreatment of the cells with the PDE3-specific inhibitor trequinsin and the PDE4-specific inhibitor rolipram (Fig. 3, *C* and *D*). PDE3 inhibition did not alter the effects of Shank2 (Fig. 3*C*). Conversely when PDE4 was inhibited by rolipram, 3 $\mu$M forskolin consistently induced a robust CFTR current in Shank2-expressing cells (Fig. 3*D*, $n = 5$), strongly suggesting an association between Shank2 and PDE4 isoforms. Recently two reports suggested that PDE4D plays a major role in forming a cAMP diffusion barrier at the apical regions of epithelial cells (22, 26). Consistent with this notion, expression of PDE4D proteins was observed in the immunob-

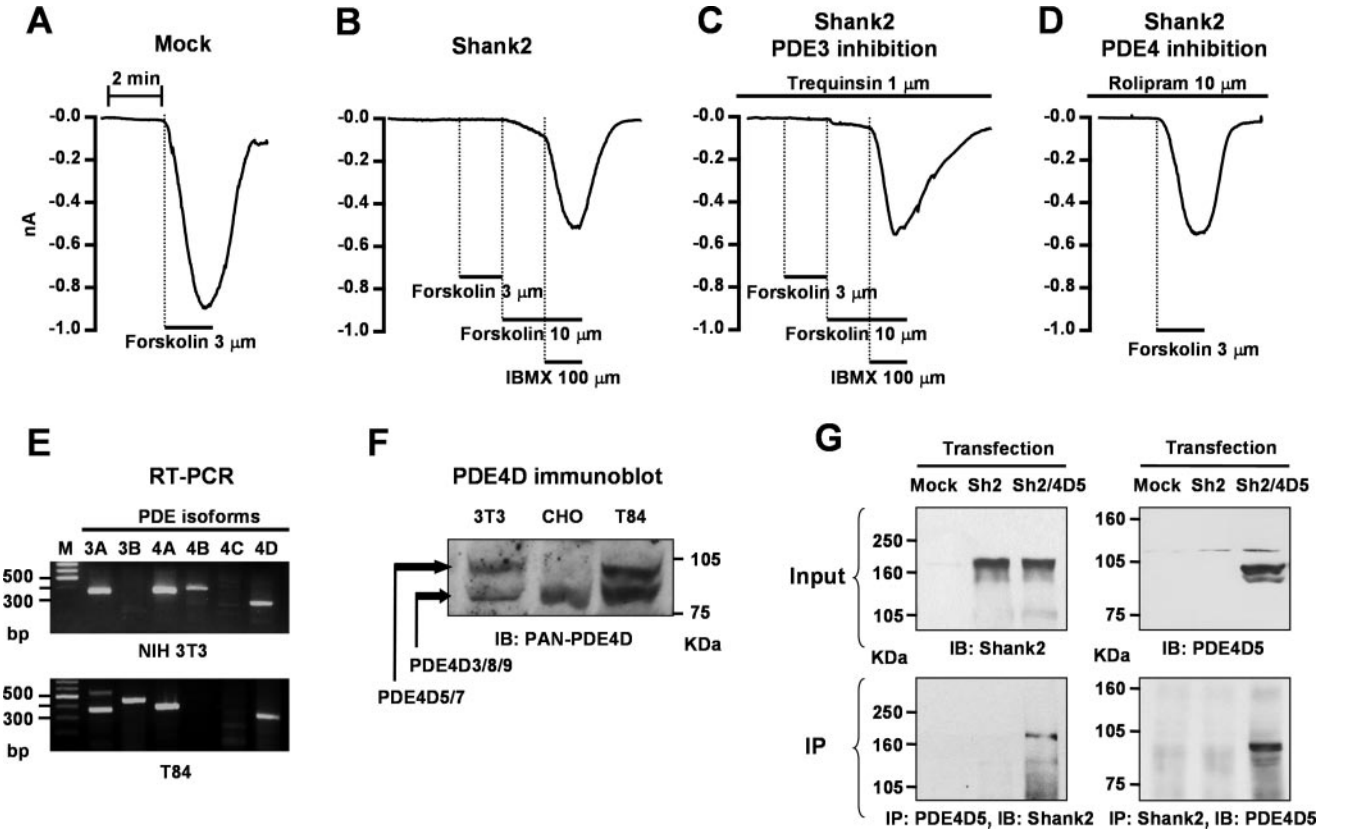


FIGURE 3. **Shank2 associates with PDE4D.** *A–D*, CFTR $Cl^-$ channel activity at whole-cell configurations was measured in CFTR-expressing CHO cells with or without Shank2 co-transfection. Treatment with forskolin (3 $\mu$M) evoked a large $Cl^-$ current in mock-transfected cells (*A*) but not in Shank2-transfected cells (*B*). CFTR currents in Shank2-transfected cells were restored by treatment with the non-selective PDE inhibitor IBMX (*B*) or the PDE4-specific inhibitor rolipram (*D*) but not with the PDE3-specific inhibitor trequinsin (*C*). *E*, detection of PDE3 and PDE4 isoforms in NIH 3T3 cells (mouse fibroblast) and T84 cells (human colonic epithelia) by reverse transcription-PCR (*RT-PCR*). Primer sequences specific to PDE3 and PDE4 isoforms were selected from the regions common to both mouse and human PDEs. *Lane M*, molecular weight markers. *F*, expression of PDE4D proteins in NIH 3T3, CHO, and T84 cells was analyzed by immunoblotting using rabbit polyclonal pan-PDE4D antibody. *G*, Shank2 (*Sh2*) and the PDE4D splice variant PDE4D5 (*4D5*) were overexpressed in CHO cells (*upper panels*) and subsequently immunoprecipitated from cell extracts using anti-PDE4D5 and anti-Shank2 antibodies (*lower panels*). *IB*, immunoblot.

lots of NIH 3T3, CHO, and T84 cells (Fig. 3*F*) in which the inhibitory effects of Shank2 on cAMP/PKA signals were demonstrated in this and previous studies (11, 12).

To probe for a physical association between Shank2 and PDE4D, co-IPs were performed. Human and rat PDE4D loci have multiple transcriptional units that code for at least nine splice variants, PDE4D1 to PDE4D9 (18). Among them, PDE4D5 has been shown to be expressed in epithelial cells and to mediate cAMP hydrolysis at the apical microdomain (22). Thus, Shank2 and the PDE4D splice variant PDE4D5 were overexpressed in CHO cells followed by IP with antibodies against Shank2 and PDE4D5 (Fig. 3*G*). Shank2 proteins were observed in immunoprecipitates with PDE4D5-specific antibodies. In a converse experiment, PDE4D5 could be detected in Shank2 immunoprecipitates. These co-IPs were specific as they could only be detected in cells expressing both Shank2 and PDE4D5 (Fig. 3*G*).

To identify its PDE4D-binding domain, several truncated Shank2 constructs were generated and used for pulldown assays. Shank2 has multiple sites for possible protein-protein interactions, including a PDZ domain, a long PR region, and a sterile $\alpha$ motif domain (27). The PR region contains five proline-rich clusters, including a cortactin-binding domain (ppI) (28). In initial pulldown assays using the lysates from the PDE4D5-transfected CHO cells, PDE4D5 showed an interaction with the PR region of Shank2 (Fig. 4*B*, *left*). The PR region was then further dissected into two parts, PR1 and PR2, and the PDE4D binding site was mapped to the PR2 region (Fig. 4*B*, *right*) where three proline-rich clusters and a ppI are clustered (Fig. 4*A*).

Next all PDE4D splice variants were co-immunoprecipitated with Shank2 to identify the PDE4D variants that interact with Shank2 and to identify the putative Shank2 binding site in PDE4D. COS-7 cells were transfected with plasmids encoding Shank2 and the nine PDE4D splice variants, PDE4D1 to PDE4D9, followed by immunoprecipitation using the pan-PDE4D antibody M3S1. All PDE4D long forms (D3, D4, D5, D7, D8, and D9) were found to interact with Shank2, whereas the short forms, D2 and D6, do not (Fig. 4*D*). A weak interaction was detected in the case of PDE4D1. The PDE4D splice variants are distinguished by the presence or absence of two conserved N-terminal domains called upstream conserved regions 1 and 2 (UCR1 and UCR2; Fig. 4*C*). The above results imply that UCR1 and the N-terminal part of UCR2 mediate Shank2 binding.

*Shank2 and PDE4D Associate in Vivo*—The association between Shank2 and PDE4D was then examined in cells that natively express both proteins to explore its physiological role.

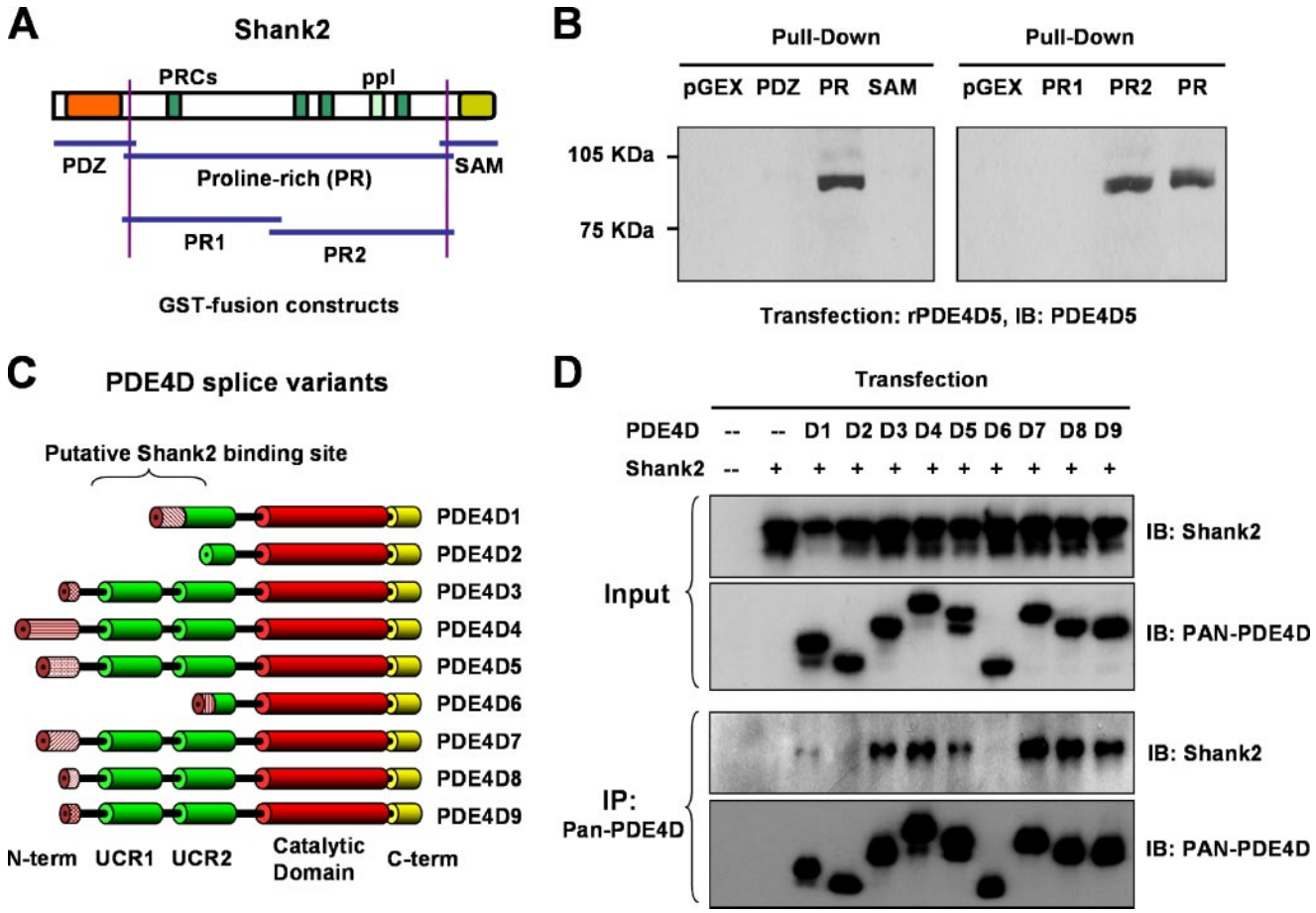


FIGURE 4. **Domains responsible for the association between Shank2 and PDE4D.** *A* and *B*, to identify the PDE4D-binding domain of Shank2, pulldown assays were performed using GST fusion proteins containing different domains of Shank2 and PDE4D expressed in CHO cells. Domain structures of the GST fusion proteins are illustrated in *A*, and pulldown results are shown in *B*. Lysates from rPDE4D5-transfected CHO cells were pulled down with GST-tagged Shank2 fragments and blotted with anti-PDE4D5 antibody. *C* and *D*, immunoprecipitation of Shank2 with the nine PDE4D splice variants. COS-7 cells were transfected with plasmids encoding Shank2 and the PDE4D splice variants, PDE4D1 to PDE4D9 (*D1–D9*). After 3 days of culture, cells were harvested, and the resulting detergent extracts were subjected to IP with the pan-PDE4D antibody M3S1. The domain structures of PDE4D splice variants are illustrated in *C*, and IP results are presented in *D*. *PRCs*, proline-rich clusters; *SAM*, sterile $\alpha$ motif; *IB*, immunoblot.

Initially we investigated the expression of Shank2 and PDE4D in rat colonic mucosa. Shank2 and PDE4D were highly co-localized at the apical region of colonic crypt cells, where CFTR plays a major role in fluid and ion secretion (Fig. 5*A*). The Shank2-PDE4D interaction was also verified by immunoprecipitation of the endogenous proteins prepared from T84 human colonic epithelial cells. It is well known that PDE4 can be activated by PKA-induced phosphorylation of UCR1 (29). Interestingly stimulation of the cAMP/PKA pathway using the adenylyl cyclase activator forskolin increased the physical association between Shank2 and PDE4D in T84 cells (Fig. 5*B*).

Finally the Shank2-PDE4D interaction was examined in mouse brain tissues where multiple PDE isoforms as well as Shank2 are expressed at high levels. In immunoprecipitates using pan-PDE4D antibodies, multiple Shank2-immunoreactive bands were detected in addition to the typical 170-kDa Shank2 (Fig. 5*C*) due to the presence of distinct Shank2 splice variants in brain tissue (17, 28). Mouse brain tissue was then immunoprecipitated with anti-Shank2 antibodies, and the resulting IP pellets were subjected to PDE activity assays. The PDE activity co-immunoprecipitating with Shank2 was inhibited by the PDE4-selective inhibitor rolipram (Fig. 5*D*). In addition, the co-immunoprecipitation of PDE was ablated in IPs using tissue from PDE4D knock-out mice (Fig. 5*E*) indicating that Shank2 specifically interacts with PDE4D in mouse brain tissue.

## DISCUSSION

In the present study, we provide comprehensive evidence that the activity of CFTR is dynamically regulated by a competitive balance between CFTR-activating and CFTR-inactivating PDZ domain interactions. In addition, activity of Shank2, the CFTR-inactivating PDZ adaptor, was found to be associated with PDE4D, which precludes cAMP/PKA signals. The regulatory mechanisms resulting from the association of CFTR with EBP50 and Shank2 are summarized in Fig. 6. It is known that EBP50 can activate CFTR through two independent mechanisms. First, EBP50 can recruit ezrin, a PKA-anchoring protein, and hence facilitates the cAMP/PKA-mediated phosphorylation of CFTR (7). Second, EBP50 can activate CFTR by conformational changes, possibly by forming a CFTR dimer (23). The results of this study revealed that Shank2 can inhibit both mechanisms by competing with EBP50 at the C terminus of CFTR. The finding that Shank2 inhibited the EBP50-induced

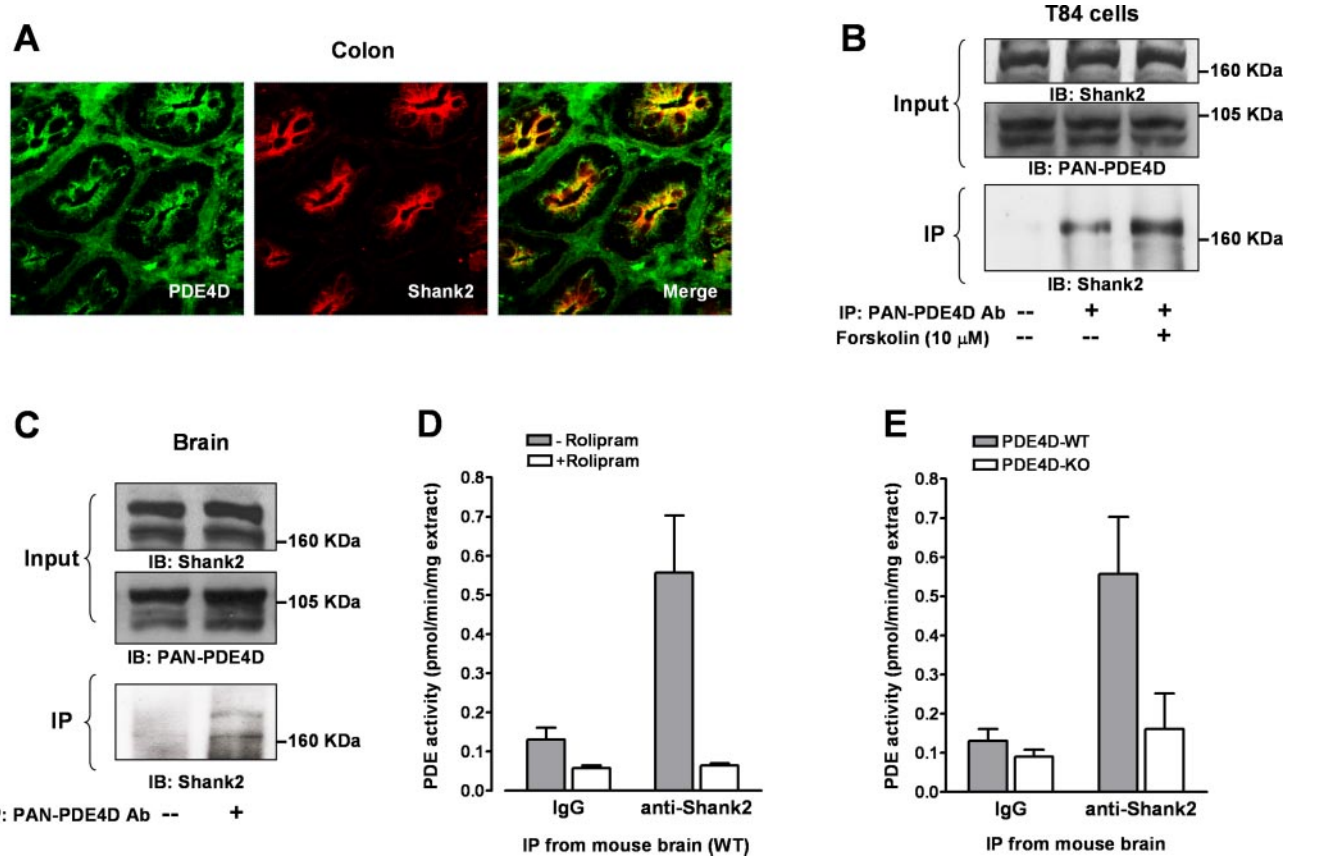


FIGURE 5. **Shank2 and PDE4D associate *in vivo*.** *A*, immunolocalization of Shank2 and PDE4D in rat colon was detected using polyclonal anti-Shank2 antibody 1136 and monoclonal pan-PDE4D antibody M3S1. Shank2 and PDE4D were co-localized in the apical region of colonic crypt cells. *B*, co-IP of Shank2 and PDE4D from extracts of human colonic T84 cells. Forskolin treatment (10 $\mu$M for 30 min) enhanced the association between Shank2 and PDE4D. *C*, detection of Shank2 proteins in PDE4D immunoprecipitates from mouse brain. *D* and *E*, measurement of PDE activity in Shank2 immunoprecipitates from mouse brain. In *D*, PDE activity in Shank2 IPs from wild type mice was determined in the presence or absence of the PDE4-specific inhibitor rolipram (10 $\mu$M). In *E*, PDE activity in immunoprecipitates from PDE4D wild type mice (*PDE4D-WT*) is compared with immunoprecipitates from PDE4D knock-out mice (*PDE4D-KO*). *Ab*, antibody; *IB*, immunoblot.

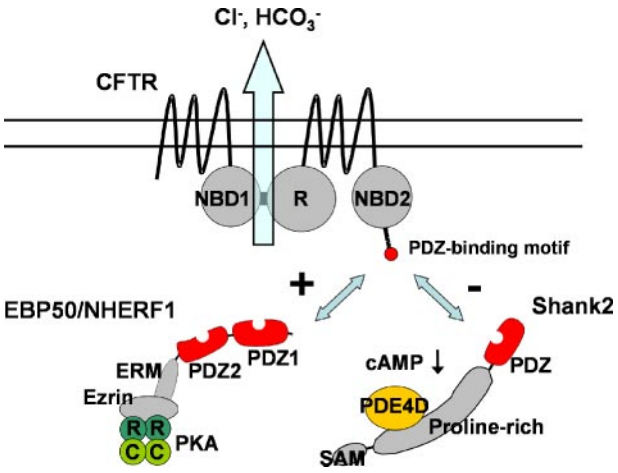


FIGURE 6. **A model for the regulation of CFTR through interaction with EBP50 and Shank2.** Through their respective PDZ domains, Shank2 and EBP50 compete for binding of the CFTR C terminus. Binding of EBP50 activates CFTR through a conformational change. In addition, EBP50 facilitates the PKA-mediated phosphorylation and activation of CFTR by bringing the AKAP ezrin and PKA into the protein complex. Shank2 inhibits CFTR activity by breaching the CFTR-EBP50 association and by bringing PDE4D, which precludes cAMP/PKA signaling, closer to CFTR. *SAM*, sterile $\alpha$ motif; *R* of CFTR, R-domain; *R* and *C* of PKA, regulatory and catalytic subunits.

increase of CFTR $P_o$ in inside-out patches (Fig. 2) demonstrated that Shank2 can antagonize the EBP50 function by breaching the EBP50-induced active conformation of CFTR independently of cAMP signals. Even more interesting, this study shows that Shank2 can ablate cAMP signaling in the vicinity of the CFTR by tethering PDE4D into this macromolecular complex.

It is well known that cAMP signals are compartmentalized in many cell types and that localized cAMP signals play a critical role in various physiological processes (29). For example, localized cAMP accumulation in a region overlapping with the Z band and the T tubules in cardiomyocytes is essential for the regulation of cardiac myocyte contraction by $\beta$-adrenergic receptors (30). Several recent reports underscored the importance of PDE4D as a cAMP diffusion barrier formed at the apical membrane of epithelia for the proper functioning of CFTR (22, 26). However, the molecular mechanisms for PDE accumulation in apical regions remained obscure. A thorough molecular characterization in this study revealed that the apical adaptor Shank2 recruits PDE4D through a direct interaction between the proline-rich region of Shank2 and the UCR1/2 region of PDE4D. The proximal localization of cAMP regulating machinery will induce an increased signaling efficiency in regulating CFTR activity. Recently Shank2E, a splice variant of Shank2 with additional ankyrin repeats and a Src homology 3 domain, was identified in epithelial cells (31). Therefore, we

repeated the experiments in Fig. 3 with Shank2E. The results were nearly identical to those obtained using Shank2 suggesting that domains within the structure of Shank2 are important for regulating CFTR function (data not shown).

The physiological significance of the Shank2-PDE4D association is not confined to epithelial cells but can be extended to other organs. For example, Shank2 is widely expressed in many regions of the brain including cortex, hippocampus, and cerebellum. Shank proteins are the key organizer of PSD and interact with Homer (27, 32), which is required for efficient signaling of metabotropic glutamate receptors that play a critical role in learning and memory. Effector systems of metabotropic glutamate receptors are not only associated with $Ca^{2+}$ signaling but also with cAMP signals, and it is believed that cAMP signals play a role in the functional specificity of each metabotropic glutamate receptor isoform (33, 34). Therefore, Shank2-associated PDE4D may play a critical role in the regulation of PSD in neuronal cells.

Recent studies with knock-out animals of NHERF family PDZ proteins (EBP50, E3KARP, and PDZK1) have shown that the functions of these adaptors are more complex than previously appreciated and appear to be tissue-specific (6). Because PDZ domains have well defined binding sites, they are promising targets for drug discovery. However, as the present study demonstrates, much is yet to be learned about the function of each PDZ-based adaptor before drugs targeting PDZ interactions can become a reality (35). For example, as the PDZ structures of EBP50 and Shank2 are very similar, small molecules or peptides targeting EBP50 may have untoward effects *in vivo* by disrupting Shank2 complexes as well.

In conclusion, the present study demonstrates the functional diversity of PDZ-mediated protein-protein interactions and illustrates that opposite signals can be delivered to the same PDZ-binding motif of a given membrane protein by different adaptors. A competitive balance between the signal-conferring and signal-stopping PDZ interactions would be critical in the regulation of many membrane transporters and receptors as demonstrated here for CFTR.

*Acknowledgments—We thank Dr. S. Muallem at the University of Texas Southwestern Medical Center and Dr. S. L. Milgram at the University of North Carolina for helpful discussions and the kind gift of the pET-EBP50 construct. We thank Caren Spencer and Kathleen Horner for editorial work on the manuscript.*

## REFERENCES

1. Sheppard, D. N., and Welsh, M. J. (1999) *Physiol. Rev.* **79,** (suppl.) S23–S45
2. Quinton, P. M. (1999) *Physiol. Rev.* **79,** (suppl.) S3–S22
3. Choi, J. Y., Muallem, D., Kiselyov, K., Lee, M. G., Thomas, P. J., and Muallem, S. (2001) *Nature* **410,** 94–97
4. Anderson, M. P., Rich, D. P., Gregory, R. J., Smith, A. E., and Welsh, M. J. (1991) *Science* **251,** 679–682
5. Chao, A. C., de Sauvage, F. J., Dong, Y. J., Wagner, J. A., Goeddel, D. V., and Gardner, P. (1994) *EMBO J.* **13,** 1065–1072
6. Lamprecht, G., and Seidler, U. (2006) *Am. J. Physiol.* **291,** G766–G777
7. Donowitz, M., Cha, B., Zachos, N. C., Brett, C. L., Sharma, A., Tse, C. M., and Li, X. (2005) *J. Physiol.* **567,** 3–11
8. Ahn, W., Kim, K. H., Lee, J. A., Kim, J. Y., Choi, J. Y., Moe, O. W., Milgram, S. L., Muallem, S., and Lee, M. G. (2001) *J. Biol. Chem.* **276,** 17236–17243
9. Funke, L., Dakoji, S., and Bredt, D. S. (2005) *Annu. Rev. Biochem.* **74,** 219–245
10. Kim, E., and Sheng, M. (2004) *Nat. Rev. Neurosci.* **5,** 771–781
11. Han, W., Kim, K. H., Jo, M. J., Lee, J. H., Yang, J., Doctor, R. B., Moe, O. W., Lee, J., Kim, E., and Lee, M. G. (2006) *J. Biol. Chem.* **281,** 1461–1469
12. Kim, J. Y., Han, W., Namkung, W., Lee, J. H., Kim, K. H., Shin, H., Kim, E., and Lee, M. G. (2004) *J. Biol. Chem.* **279,** 10389–10396
13. Weinman, E. J., Steplock, D., Wang, Y., and Shenolikar, S. (1995) *J. Clin. Investig.* **95,** 2143–2149
14. Yun, C. H., Lamprecht, G., Forster, D. V., and Sidor, A. (1998) *J. Biol. Chem.* **273,** 25856–25863
15. Taouil, K., Hinnrasky, J., Hologne, C., Corlieu, P., Klossek, J. M., and Puchelle, E. (2003) *J. Biol. Chem.* **278,** 17320–17327
16. Im, Y. J., Lee, J. H., Park, S. H., Park, S. J., Rho, S. H., Kang, G. B., Kim, E., and Eom, S. H. (2003) *J. Biol. Chem.* **278,** 48099–48104
17. Lim, S., Naisbitt, S., Yoon, J., Hwang, J. I., Suh, P. G., Sheng, M., and Kim, E. (1999) *J. Biol. Chem.* **274,** 29510–29518
18. Richter, W., Jin, S. L., and Conti, M. (2005) *Biochem. J.* **388,** 803–811
19. Namkung, W., Kim, K. H., and Lee, M. G. (2005) *Gastroenterology* **129,** 1979–1990
20. Iona, S., Cuomo, M., Bushnik, T., Naro, F., Sette, C., Hess, M., Shelton, E. R., and Conti, M. (1998) *Mol. Pharmacol.* **53,** 23–32
21. Jin, S. L., Richard, F. J., Kuo, W. P., D'Ercole, A. J., and Conti, M. (1999) *Proc. Natl. Acad. Sci. U. S. A.* **96,** 11998–12003
22. Barnes, A. P., Livera, G., Huang, P., Sun, C., O'Neal, W. K., Conti, M., Stutts, M. J., and Milgram, S. L. (2005) *J. Biol. Chem.* **280,** 7997–8003
23. Raghuram, V., Mak, D. D., and Foskett, J. K. (2001) *Proc. Natl. Acad. Sci. U. S. A.* **98,** 1300–1305
24. Wang, S., Yue, H., Derin, R. B., Guggino, W. B., and Li, M. (2000) *Cell* **103,** 169–179
25. Mehats, C., Andersen, C. B., Filopanti, M., Jin, S. L., and Conti, M. (2002) *Trends Endocrinol. Metab.* **13,** 29–35
26. Liu, S., Veilleux, A., Zhang, L., Young, A., Kwok, E., Laliberte, F., Chung, C., Tota, M. R., Dube, D., Friesen, R. W., and Huang, Z. (2005) *J. Pharmacol. Exp. Ther.* **314,** 846–854
27. Sheng, M., and Kim, E. (2000) *J. Cell Sci.* **113,** 1851–1856
28. Boeckers, T. M., Bockmann, J., Kreutz, M. R., and Gundelfinger, E. D. (2002) *J. Neurochem.* **81,** 903–910
29. Conti, M., Richter, W., Mehats, C., Livera, G., Park, J. Y., and Jin, C. (2003) *J. Biol. Chem.* **278,** 5493–5496
30. Zaccolo, M., and Pozzan, T. (2002) *Science* **295,** 1711–1715
31. McWilliams, R. R., Gidey, E., Fouassier, L., Weed, S. A., and Doctor, R. B. (2004) *Biochem. J.* **380,** 181–191
32. Tu, J. C., Xiao, B., Naisbitt, S., Yuan, J. P., Petralia, R. S., Brakeman, P., Doan, A., Aakalu, V. K., Lanahan, A. A., Sheng, M., and Worley, P. F. (1999) *Neuron* **23,** 583–592
33. Francesconi, A., and Duvoisin, R. M. (2000) *Proc. Natl. Acad. Sci. U. S. A.* **97,** 6185–6190
34. Tateyama, M., and Kubo, Y. (2006) *Proc. Natl. Acad. Sci. U. S. A.* **103,** 1124–1128
35. Dev, K. K. (2004) *Nat. Rev. Drug Discov.* **3,** 1047–1056